ACS APPLIED MATERIALS & INTERFACES

Letter

www.acsami.org

Electrochemical Performance of Electrodeposited Zn_4Sb_3 Films for Sodium-Ion Secondary Battery Anodes

E. D. Jackson, S. Green, and A. L. Prieto*

Department of Chemistry, Colorado State University, Fort Collins, Colorado, United States

Supporting Information

ABSTRACT: We report the electrodeposition of zinc−antimony composite films from aqueous solution. We show that it is possible to produce Zn_4Sb_3 films on zinc substrates by low-temperature annealing and we evaluate their performance as sodium-ion battery anodes. Near complete utilization of the antimony (>90%) during cycling, good cycle life (>250 cycles), and high rate performance is demonstrated for Zn_4Sb_3 thin films. Interestingly, when Zn_4Sb_3 transforms in situ to an amorphous zinc−antimony composite, it shows superior performance to zinc−antimony composites that are initially amorphous. This demonstrates the importance of the initial electrode structure on promoting the sodium alloying reaction.

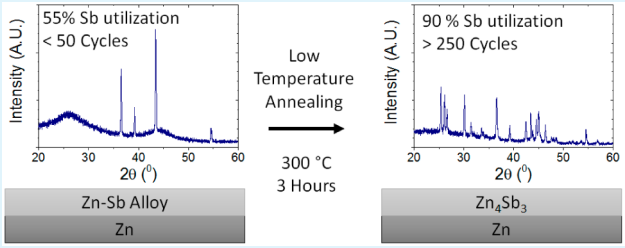

KEYWORDS: *zinc antimonide, sodium-ion battery, thin film anode, electrodeposition*

Sodium-ion batteries have recently regained significant interest as an alternative to lithium-ion batteries. As opposed to lithium, sodium is advantageous because of higher abundance, good global distribution, lower cost, a standard reduction potential near that of lithium (−3.04 V for Li/Li^+ and −2.71 V for Na/Na^+), and the potential for new cell chemistries impractical with lithium. Although the theoretical energy and power densities of a sodium battery are lower than the lithium analogue, sodium batteries may become important for stationary and grid applications where inexpensive rechargeable batteries are needed.

The amount of research on potential anode materials for secondary sodium-ion batteries has been fairly limited, and low-cost negative electrode materials with high energy density are required in order to make a sodium-ion battery economically viable. The high reactivity of sodium with air and water make it an unattractive negative electrode due to safety concerns. Fortuitously, it has been observed that in many cases sodium undergoes similar electrochemical reactions as lithium and analogues of lithium-ion negative electrodes are therefore clear candidates for sodium-ion batteries. Analogous to lithium ion anode targets, metal-based sodium ion battery anode targets are attractive because of their good voltage characteristics and high theoretical capacity, and include Si (954 mAh g^{-1}), Sn (847 mAh g^{-1}), and Sb (660 mAh g^{-1}).[1]

Antimony in particular has been investigated because of its high theoretical capacity, good kinetic performance, and voltage characteristics.[2−5] One would think that sodium negative electrodes (as compared to lithium) would experience faster capacity fade because of the larger size of sodium ions, contributing to greater volume changes and faster pulverization.[1] Unexpectedly, substantially better cycle life has been reported for reversible sodiation and desodiation reactions, in contrast to the poor cycle life of pure antimony with lithium.[6,7] Additionally, the phases produced during sodium insertion do not appear to follow the thermodynamically predicted intermediates based on phase diagrams, and instead often proceed via amorphous intermediates. This has led to additional interest in high-capacity anodes that are not possible in lithium-ion batteries because of pulverization.

Alloys of antimony have also been investigated, either to further increase capacity retention or offer other benefits, such as improved electrical conductivity and better mechanical properties. In addition to pure antimony, Sb_2O_4,[8] SnSb,[9,10] Cu_2Sb,[11] and Cu_6Sn_5,[12] as well as some other alloy-based composites,[13−15] have been investigated as potential anode candidates. A common theme among all of these anodes is their ability to cycle for at least several cycles, despite the very large volume expansion and contraction that occurs during cycling.

Here we report the use of zinc as an alloying element to improve the electrochemical performance of antimony as a sodium ion battery anode material. Zinc is interesting because of its' high abundance, low cost, and good conductivity. Additionally, unlike lithium, sodium does not react electrochemically with zinc. As a result, it can be utilized both as a substrate material and as an additive for the anode electrode. These properties are advantageous for the sodium-ion battery, where low materials and manufacturing costs are critical considerations.

We have synthesized Zn_4Sb_3 and Zn−Sb alloy films with varying zinc content by the electrodeposition of antimony onto zinc substrates using a pH neutral aqueous gluconate-chloride

Received: November 18, 2014
Accepted: February 2, 2015
Published: February 2, 2015

DOI: 10.1021/am507436u
ACS Appl. Mater. Interfaces 2015, 7, 7447−7450

electrolyte (cyclic voltammograms shown and discussed in Figure S1 in the Supporting Information). Gluconate acts both as a complexing agent and electrode surfactant, allowing the codeposition of amorphous zinc antimonide without excessive hydrogen gas formation. Additionally, the neutral pH suppresses either element from preferentially depositing and creating a heterogeneous or dendritic deposit (see Figure S2 in the Supporting Information). Using a very high overpotential, films with low amounts of oxygen are obtained with a zinc to antimony ratio the same as the ratio of the dissolved metal chloride salt concentrations in the electrolyte bath (see Figure S3 in the Supporting Information). Adherent, flat, and silvery thin films are obtained with good homogeneity.

Amorphous deposits are obtained initially, allowing the investigation of zinc-doped antimony alloy films (see Figure S4 in the Supporting Information). Initial cycling data of these films indicate two major charge potential plateaus and a sloping discharge potential profile (see Figure S5 in the Supporting Information). The two charging plateaus become more distinct upon additional cycling and are easily distinguished in the second cycle. The discharge potential profile only changes slightly, with no well-defined plateaus. Surprisingly, the incorporation of zinc has no major effect on the potential profile of the antimony, with little difference between the samples with up to 50 mol % zinc and zinc-free deposits. This is likely due to the amorphous nature of the deposit, causing the electrochemically inactive zinc to operate as a by-stander in the reaction. Prior to annealing, these films show only modest performance and exhibit rapid capacity fading (see Figure S6 in the Supporting Information).

To achieve enhanced performance, we annealed the Zn−Sb amorphous films under argon to form crystalline Zn_4Sb_3. We chose to use deposits with an initial zinc to antimony ratio of 2:3, allowing annealing time to be balanced with substrate to film diffusion and to allow a lower diffusion temperature. Prior to annealing, we analyzed the cross-section of these films by SEM to determine the approximate film thicknesses (see Figure S7 in the Supporting Information). The approximate average thicknesses were found to be 200 nm, 450 nm, and 780 for deposition times of 2, 6, and 10 min, respectively. These values correspond well to thicknesses estimated using the average density of antimony and zinc metal and the mass of the deposited material. The corresponding mass loading of the electrodes were 122, 274, and 474 μg cm^{-2}. These results indicate that the films have good homogeneity and are clearly smooth and nonporous.

Annealing conditions were optimized to form high-quality Zn_4Sb_3 films. It was found that annealing zinc-deficient films deposited from a 2:3 Zn:Sb solution on zinc substrates at a temperature of 300 °C under 700 Torr argon for 3 h resulted in high intensity peaks corresponding to Zn_4Sb_3 (Figure 1). Lower temperatures resulted in poor crystallinity, whereas higher temperatures degraded the film by the formation of very small nanowires (not shown) and low intensity diffraction peaks representing Zn_4Sb_3, a phenomenon that has been reported previously.[16] The effect of annealing time was also examined on both 2 and 10 min depositions to ensure the annealing conditions were adequate for a range of different film thicknesses (see Figure S8 in the Supporting Information). It was found that 6 h was optimal for 10 min depositions, but annealing over 3 h for 2 min depositions led to an excess of zinc at the surface.

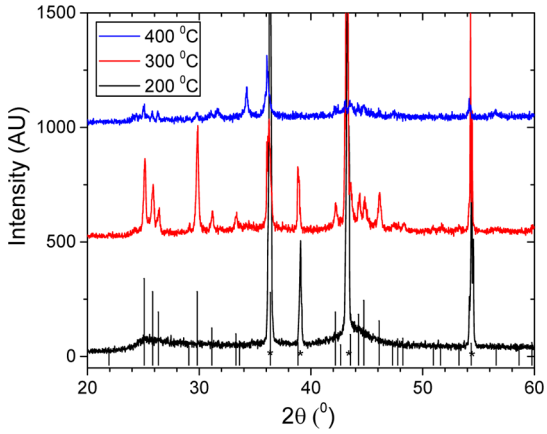

Figure 1. Glancing incident X-ray diffraction patterns of 10 min depositions from a 20 mM $ZnCl_2$ deposition solution annealed at 200−400 °C for 3 h. Peaks marked with an asterisk are from the zinc substrate. All other peaks correspond to Zn_4Sb_3 (PDF 00−056−1306). All scans were taken at 1° incident angle.

The electrochemical performance of these Zn_4Sb_3@Zn anodes were evaluated in sodium half cells (Figure 2). A high

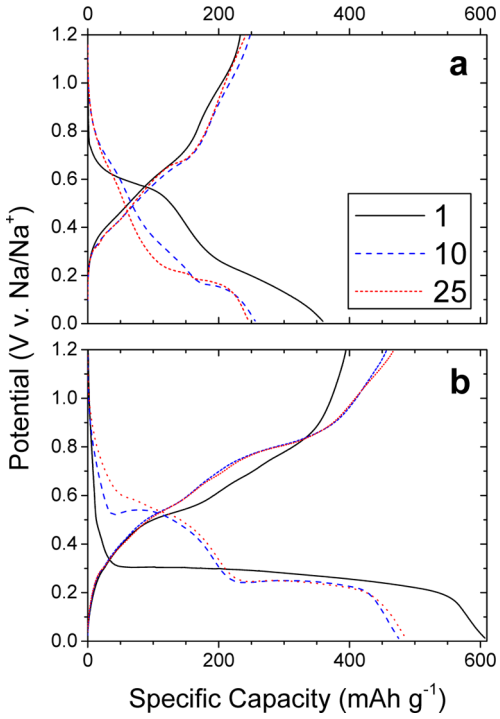

Figure 2. Charge−discharge voltage profiles for the 1st (black solid), 10th (blue dashed), and 25th (red dotted) cycles for (a) an amorphous 4:3 Zn:Sb thin film deposited for 240 s and (b) an annealed 2:3 Zn:Sb thin film annealed for 6 h at 300 °C under argon to produce Zn_4Sb_3. Films were cycled in a sodium-ion cell between 0.01 and 1.20 V. The electrolyte used is 1 M $NaClO_4$ in PC with 5% FEC additive.

capacity of 450 mAh g^{-1} is near to the theoretical capacity of 486 mAh g^{-1} for a film deposited from a 2:3 Zn:Sb solution. Once corrected for two additional stoichiometric equivelents of zinc introduced during annealing, this gives a reversible capacity of 357 mAh g^{-1}. Unlike the case for zinc incorporation into amorphous antimony films, the formation of crystalline Zn_4Sb_3 causes a significant change in the initial potential profiles of the

DOI: 10.1021/am507436u
ACS Appl. Mater. Interfaces 2015, 7, 7447−7450

electrode during both sodium insertion and desertion. The sloping sodium incorporation profile seen in amorphous deposits is replaced with a single, well-defined potential plateau at ~0.3 V v. Na/Na^+. The discharge profile of the annealed films are initially not distinguishably different from the amorphous films, displaying a sloped profile with no well-defined plateaus. Upon subsequent cycles, a new distinct charge plateau appears at ~0.5 V v. Na/Na^+, resulting in a clear two-step charge profile at 10 cycles that gradually becomes less distinct with prolonged cycling. Similarly, at ten cycles there is a clear discharge plateau that is present at 0.8 V v. Na/Na^+ that is not seen when initially amorphous films are used. Although we were unable to resolve any unique phases during the charge–discharge process using ex situ XRD, the two-plateau charge mechanism is distinct for Zn_4Sb_3 versus the amorphous material and is likely critical to the improved performance.

Cyclic voltammetry was performed in a half cell configuration with a Zn_4Sb_3 electrode and sodium counter electrode (Figure 3a). An initial single cathodic peak that occurs at

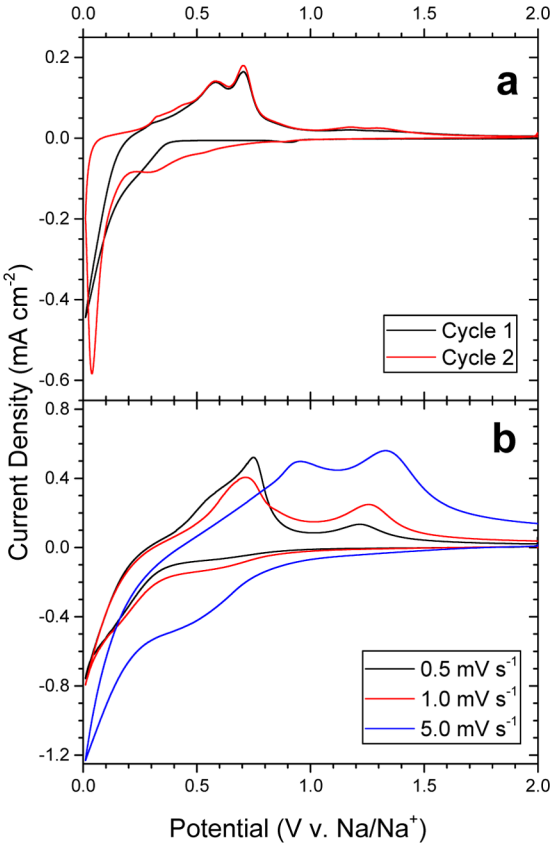

Figure 3. Cyclic voltammetry of an annealed Zn_4Sb_3 electrode in a half-cell configuration with a sodium counter electrode as a function of (a) cycle number and (b) scan rate.

potentials below 0.3 V indicates a clear one-step sodium conversion on the first cycle. Upon reversal, two anodic peaks at 0.55 and 0.70 V are present, suggesting a more complex reaction to remove sodium. A minor third anodic peak is present at a relatively high voltage of 1.25 V. The second cycle shows the development of a higher potential cathodic peak that starts at 0.50 V and reaches maximum current at 0.30 V. An additional cathodic peak is present at 0.30 V. These two additional peaks are the result of the in situ formation of an amorphous zinc–antimony composite that occurs because of the in situ conversion reaction of sodium with Zn_4Sb_3. Subsequent cyclic voltammograms do not show further changes in the film electrochemistry. The kinetic performance of Zn_4Sb_3 thin films is exceptional, with ~300 nm films providing 325 mAh g^{-1} at a discharge rates of up to 2C and 275 mAh g^{-1} at 10C (see Figure S9 in the Supporting Information). This good performance is likely facilitated by the thin film thickness, but these high capacities show that this material has good kinetic properties that enable high rates when lithium diffusion lengths are short. We noticed a substantial change in the shape of the charge and discharge profiles at fast rates. We consider the good high rate performance to be in part due to this change in electrode electrochemistry. To study this phenomena, we performed cyclic voltammograms at increased rates (Figure 3b). As expected, the anodic peaks become polarized to higher potentials, reaching 0.95 V at a 5 mV s^{-1} scan rate. Unexpectedly, the previously very small anodic peak at 1.25 V greatly increases in magnitude until it is larger than the low potential anodic peaks. This suggests that the high rate performance may be the result of a fast conversion process that becomes activated when the polarization is large. This mechanism accounts for unexpected good rate performance of Zn_4Sb_3. Further exploration of this mechanism is required to definitely determine the conversion mechanism of the material.

Annealed films display superior cycle life compared to amorphous films, with thin films (~200–400 nm) retaining over 90% of their maximum capacity for over 250 cycles (Figure 4). In contrast, thick electrodes over ca. 600 nm display

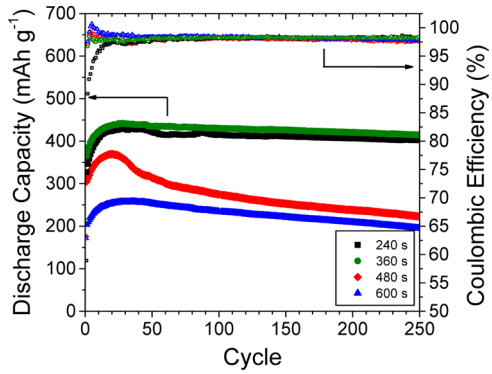

Figure 4. Cycle life performance of annealed Zn_4Sb_3 thin films annealed for 3 h at 300 °C cycled in sodium half-cells at a C/5 rate.

both lower reversible capacity and shorter cycle life. Pulverization appears to be significantly worse for thicker electrodes, where electrode cracking occurs even on the first cycle (see Figure S10 in the Supporting Information). Regardless of the thickness, an initial Coulombic efficiency of ~60% is obtained, with efficiencies >95% after the first few cycles. The Zn_4Sb_3 films maintain above 98% efficiency after the first five cycles.

It is important to note that although both the Zn–Sb amorphous deposits and crystalline Zn_4Sb_3 form an amorphous material upon cycling, they exhibit significantly different electrochemical performance. The amorphous deposit is capable of reversibly reacting with only 55–65% of the antimony, whereas the crystalline Zn_4Sb_3 deposit uses more than 90% of the available antimony. Additionally, the utilization of a higher amount of antimony in the deposit would normally imply that the crystalline deposits undergo faster pulverization and capacity loss. We ascribe these differences to the ability of

DOI: 10.1021/am507436u
ACS Appl. Mater. Interfaces 2015, 7, 7447–7450

Zn_4Sb_3 to react directly with sodium ions to produce the Na_3Sb product across the entire electrode, while simultaneously extruding zinc in such a way that it does not impair sodium ion transfer. The homogeneous nature of the crystalline deposits reduces local variations in zinc concentrations, and therefore all the antimony is available for reaction. In contrast, the amorphous deposits may have local areas that are extremely zinc-rich, effectively trapping portions of antimony such that they cannot be accessed by sodium ions and creating volumes of material that are effectively inactive. This illustrates the importance of atomic-level order on the reversibility of Zn_4Sb_3 in sodium-ion batteries.

In conclusion, we have studied the behavior of amorphous zinc−antimony alloys and annealed Zn_4Sb_3 using electrodeposited thin films. The potential profile between 0.10 and 1.20 V is within the useful range for nonaqueous rechargeable sodium-ion anode materials. While amorphous zinc−antimony thin films display poor anode performance, annealed thin films of crystalline Zn_4Sb_3 show superior cycle life, high efficiency, and a high capacity. The use of zinc as an alloying agent and substrate is important. Although zinc is less conductive than the copper currently used in lithium-ion batteries, zinc is both inexpensive and abundant. As a result, this system is of practical interest for applications where low cost and good long-term performance are more important factors than high energy and power density.

■ ASSOCIATED CONTENT

Ⓢ Supporting Information

Experimental details. This material is available free of charge via the Internet at http://pubs.acs.org.

■ AUTHOR INFORMATION

Corresponding Author

*E-mail: alprieto@lamar.colostate.edu.

Funding

This research was supported by the NSF CAREER grant DMR-0956011.

Notes

The authors declare no competing financial interest.

■ ACKNOWLEDGMENTS

The authors gratefully acknowledge the assistance of CSU staff scientists Dr. Brian Newell with XRD experiments and Dr Pat McCurdy with SEM experiments.

■ ABBREVIATIONS

FEC, fluoroethylene Carbonate
SEI, surface electrolyte interface
Zn_4Sb3, zinc antimonide
XRD, X-ray diffraction

■ REFERENCES

(1) Chevrier, V. L.; Ceder, G. Challenges for Na-ion Negative Electrodes. *J. Electrochem. Soc.* **2011**, *158*, A1011−A1014.

(2) Darwiche, A.; Marino, C.; Sougrati, M. T.; Fraisse, B.; Stievano, L.; Monconduit, L. Better Cycling Performances of Bulk Sb in Na-Ion Batteries Compared to Li-Ion Systems: An Unexpected Electrochemical Mechanism. *J. Am. Chem. Soc.* **2012**, *134*, 20805−20811.

(3) Hou, H.; Jing, M.; Yang, Y.; Zhu, Y.; Fang, L.; Song, W.; Pan, C.; Yang, X.; Ji, X. Sodium/Lithium Storage Behavior of Antimony Hollow Nanospheres for Rechargeable Batteries. *ACS Appl. Mater. Interfaces* **2014**, *6*, 16189−16196.

(4) He, M.; Kravchyk, K.; Walter, M.; Kovalenko, M. V. Monodisperse Antimony Nanocrystals for High-Rate Li-ion and Na-ion Battery Anodes: Nano versus Bulk. *Nano Lett.* **2014**, *14*, 1255−1262.

(5) Baggetto, L.; Ganesh, P.; Sun, C.-N.; Meisner, R. A.; Zawodzinski, T. A.; Veith, G. M. Intrinsic Thermodynamic and Kinetic Properties of Sb Electrodes for Li-ion and Na-ion Batteries: Experiment and Theory. *J. Mater. Chem. A* **2013**, *1*, 7985−7994.

(6) Qian, J.; Chen, Y.; Wu, L.; Cao, Y.; Ai, X.; Yang, H. High Capacity Na-storage and Superior Cyclability of Nanocomposite Sb/C Anode for Na-ion Batteries. *Chem. Commun.* **2012**, *48*, 7070−7072.

(7) Baggetto, L.; Ganesh, P.; Sun, C.-N.; Meisner, R. A.; Zawodzinski, T.; Veith, G. M. Intrinsic Thermodynamic and Kinetic Properties of Sb Electrodes for Li-ion and Na-ion Batteries: Experiment and Theory. *J. Mater. Chem. A* **2013**, *1*, 7985−7994.

(8) Sun, Q.; Ren, Q.-Q.; Li, H.; Fu, Z.-W. High capacity Sb_2O_4 Thin Film Electrodes for Rechargeable Sodium Battery. *Electrochem. Commun.* **2011**, *13*, 1462−1464.

(9) Darwiche, A.; Sougrati, M. T.; Fraisse, B.; Stievano, L.; Monconduit, L. Facile Synthesis and Long cycle Life of SnSb as Negative Electrode Material for Na-ion Batteries. *Electrochem. Commun.* **2013**, *32*, 18−21.

(10) Xiao, L.; Cao, Y.; Xiao, J.; Wang, W.; Kovarik, L.; Nie, Z.; Liu, J. High Capacity, Reversible Alloying Reactions in SnSb/C Nanocomposites for Na-ion battery Applications. *Chem. Commun.* **2012**, *48*, 3321−3323.

(11) Baggetto, L.; Allcorn, E.; Manthiram, A.; Veith, G. M. Cu_2Sb Thin Films as Anode for Na-ion Batteries. *Electrochem. Commun.* **2013**, *27*, 168−171.

(12) Baggetto, L.; Jumas, J.-C.; Gorka, J.; Bridges, C. A.; Veith, G. M. Predictions of Particle Size and Lattice Diffusion Pathway Requirements for Sodium-ion Anodes using η-Cu_6Sn_5 Thin Films as a Model System. *Phys. Chem. Chem. Phys.* **2013**, *15*, 10885−10894.

(13) Wu, L.; Pei, F.; Mao, R.; Wu, F.; Wu, Y.; Qian, J.; Cao, Y.; Ai, X.; Yang, H. SiC-Sb-C Nanocomposites as High-Capacity and Cycling-Stable Anode for Sodium-ion Batteries. *Electrochim. Acta* **2012**, *87*, 41−45.

(14) Kim, I. T.; Allcorn, E.; Manthiram, A. High-Performance M_xSb−Al_2O_3−C (M= Fe, Ni, and Cu) Nanocomposite-Alloy Anodes for Sodium-Ion Batteries. *Energy Technology* **2013**, *1*, 319−326.

(15) Baggetto, L.; Allcorn, E.; Unocic, R. R.; Manthiram, A.; Veith, G. M. Mo_3Sb_7 as a Very Fast Anode Material for Lithium-ion and Sodium-ion Batteries. *J. Mater. Chem. A* **2013**, *1*, 11163−11169.

(16) Liu, P.; Guo, X.; Huang, H.; Yang, Q.; Tong, Y.; Hope, G. A. The Growth of Zn−Sb Nanowires by Heat Treatment of Zn−Sb Nanoparticles Obtained by Electrodeposition. *Adv. Mater.* **2006**, *18*, 1873−1876.

DOI: 10.1021/am507436u
ACS Appl. Mater. Interfaces 2015, 7, 7447−7450